Quantifying the distribution of nanodiamonds in pre-Younger Dryas to recent age deposits along Bull Creek, Oklahoma Panhandle, USA

Leland C. Bement[a,1], Andrew S. Madden[b], Brian J. Carter[c], Alexander R. Simms[d], Andrew L. Swindle[b], Hanna M. Alexander[d], Scott Fine[c], and Mourad Benamara[e]

[a]Oklahoma Archeological Survey and [b]School of Geology and Geophysics, University of Oklahoma, Norman, OK 73019; [c]Department of Plant and Soil Sciences, Oklahoma State University, Stillwater, OK 74078; [d]Department of Earth Science, University of California, Santa Barbara, CA 93106; and [e]Institute for Nanoscience and Engineering, University of Arkansas, Fayetteville, AR 72701

Edited by Henry J. Melosh, Purdue University, West Lafayette, IN, and approved December 23, 2013 (received for review May 22, 2013)

High levels of nanodiamonds (nds) have been used to support the transformative hypothesis that an extraterrestrial (ET) event (comet explosion) triggered Younger Dryas changes in temperature, flora and fauna assemblages, and human adaptations [Firestone RB, et al. (2007) *Proc Natl Acad Sci USA* 104(41):16016–16021]. We evaluate this hypothesis by establishing the distribution of nds within the Bull Creek drainage of the Beaver River basin in the Oklahoma panhandle. The earlier report of an abundance spike of nds in the Bull Creek I Younger Dryas boundary soil is confirmed, although no pure cubic diamonds were identified. The lack of hexagonal nds suggests Bull Creek I is not near any impact site. Potential hexagonal nds at Bull Creek were found to be more consistent with graphene/graphane. An additional nd spike is found in deposits of late Holocene through the modern age, indicating nds are not unique to the Younger Dryas boundary. Nd distributions do not correlate with depositional environment, pedogenesis, climate perturbations, periods of surface stability, or cultural activity.

North American Southern Plains | megafauna extinction

A recent hypothesis states that an extraterrestrial (ET) collision triggered the Younger Dryas (YD) chronozone ~10,900 ± 100 radiocarbon years before present (RCYBP) and left event-specific markers, including magnetic grains with iridium, magnetic microspherules, charcoal, soot and polycyclic hydrocarbons, carbon spherules, glass-like carbon, nanodiamonds (nds), and fullerenes with ET helium (1). Opponents of this hypothesis point to the need for outside corroboration of the presence of "above-background levels" of certain markers, including nds (2, 3). In addition, event-marker concentrations need to be quantified in deposits of other periods. This approach requires both the testing of stratified samples immediately above and below those containing ET markers, as reported by Firestone and coworkers (1) and Kennett and colleagues (4), and the search for concentrations of ET markers in similar deposits of other periods to eliminate depositional congruence as the mode of concentrating markers into higher-than-background levels.

Reproducibility and interpretations of various ET markers have proven to be extremely controversial (e.g., refs. 5–10). Nds are no exception: their various phases [cubic, n-diamond, hexagonal (hex)], incredibly tiny size, and similarity to other carbon forms has led to seemingly conflicting reports regarding the identity and distribution of nds in and near YD sediments (e.g., refs. 4, 7, and 11–16). The YD signature afforded by the stable carbon isotope record within the Bull Creek (BC) study area of northwestern Oklahoma (17) attracted ET proponents who then discovered a concentration of cubic nds in two adjacent samples at the YD boundary (YDB) BCI sediments, but not in deposits below or above them (4).

Nanodiamond investigations separate from those of the original Firestone group produced mixed results. Daulton and colleagues (12) reported "No evidence of nds in Younger-Dryas sediments," but their investigation was limited to only crushed "microcharcoal aggregates" from the Murray Springs, Arizona, site. Tian and coworkers (14) identified cubic diamonds in a YD-equivalent layer in Belgium. van Hoesel and colleagues (7) identified cubic nds in glassy carbon, but at a stratigraphic layer approximately 200 y after the YD onset. Neither Daulton and colleagues (12) nor van Hoesel and coworkers (7) examined whole-sediment digestions.

Because nds are one of the proposed ET event markers and have already been reported from the study area, we investigated nd distributions in soils and sediments of the BC valley to address the following questions: What is the spatial, temporal, pedologic, and lithostratigraphic distribution of nds in the BC area? What bearing does this distribution have on the ET hypothesis?

The BC area is centrally located in the Great Plains and is ideally suited for additional intensive investigation (*SI Appendix*, Fig. S1.1). Addressing research questions requires sampling several sites in the BC area and testing for nd concentrations in soils and sediments similar to those at BCI. Criteria used in selecting test profiles included, but were not limited to, similar depositional environment, lithostratigraphy, pedogenic characteristics, and global climatic setting at the time of soil formation (in particular, global atmospheric dynamics). Natural agents that concentrate materials on a surface or within soils and sediments include alluvial, colluvial, and aeolian deposition; surface deflation; pedogenesis; and possible anthropogenic factors.

The foundation for this project was provided by the recent results of multiproxy analyses from the BCI site (18, 19) and the projected expansion to additional key sites in this area. Through a combination of particle size distribution, stable carbon

Significance

In 2007, scientists proposed that the start of the Younger Dryas (YD) chronozone (10,900 radiocarbon years ago) and late Pleistocene extinctions resulted from the explosion of a comet in the earth's atmosphere. The ET event, as it is known, is purportedly marked by high levels of various materials, including nanodiamonds. Nanodiamonds had previously been reported from the Bull Creek, Oklahoma, area. We investigate this claim here by quantifying the distribution of nanodiamonds in sediments of different periods within the Bull Creek valley. We found high levels of nanodiamonds in YD boundary deposits, supporting the previous claim. A second spike in nanodiamonds during the late Holocene suggests that the distribution of nanodiamonds is not unique to the YD.

Author contributions: L.C.B., A.S.M., B.J.C., and A.R.S. designed research; L.C.B., A.S.M., B.J.C., A.R.S., A.L.S., H.M.A., and S.F. performed research; L.C.B., A.S.M., B.J.C., A.R.S., A.L.S., H.M.A., S.F., and M.B. analyzed data; and L.C.B., A.S.M., B.J.C., and A.R.S. wrote the paper.

The authors declare no conflict of interest.

This article is a PNAS Direct Submission.

[1]To whom correspondence should be addressed. E-mail: Lbement@ou.edu.

This article contains supporting information online at www.pnas.org/lookup/suppl/doi:10.1073/pnas.1309734111/-/DCSupplemental.

isotopes, pollen, phytolith, and biostratigraphic analyses, the paleoenvironment from roughly 11,000 to 6,000 RCYBP has been reconstructed (*SI Appendix*, Fig. S1.2) (18).To assess the possibility that concentrations of nds might be present in sediments of other ages, sites with characteristics similar to those at BCI but of earlier and later ages were selected. These additional site localities span other YD-like climatic events such as Bond cycles (Holocene rapid climate change events, including the 8.2-ka event) (20, 21), Dansgaard–Oeschger (DO) cycles of Late Pleistocene rapid climate change events (22, 23), and Heinrich events (24). The profile at BCI meets the requirements for later-age deposits and possible correlation to Bond cycles and Heinrich events, including soils with ages at ∼10,400, ∼9,850, ∼8,670, ∼7,660, and ∼6,200 RCYBP.

On the basis of what we know for buried soils at BCI, their paleosurface stability is cumulic and accompanied by reduced sedimentation rates and soil development. If nd concentrations accrue on these surfaces, then samples from each of the soil A horizons with thicknesses and length of development equal to or greater than that displayed in the sample where Kennett and colleagues (4) identified a spike in nd quantities (∼11,000 RCYBP) should contain comparable or greater densities of nds. One of these soils is easily seen along BC and neighboring drainages.

The upper limit of this roughly 100-cm-thick soil consistently dates to ∼10,280 RCYBP and displays the greatest period of continuous pedogenesis in the BC and surrounding drainages (19), with a deposition rate of 0.17 cm/year. If nd densities are linked to pedogenesis, then greater frequencies should be found in the ∼10,280 RCYBP soil than reside in the ∼11,000 RCYBP soil. Later deposition in the valley is aeolian in nature, with small increments of deposition (0.028 cm/y) from ∼9,800 to 6,200 RCYBP. Soils formed in these aeolian deposits along BC represent six times the stability seen in the alluvial deposits. Accrual of nds on the latest aeolian surfaces should be even greater, with deposition rates of only 0.0074 cm/y, representing 23 times the surface stability displayed in alluvial soils. Again, these aeolian soils should contain nd frequencies in excess to those identified in the ∼11,000-y-old soil formed in alluvium if nd frequency is tied to relative surface stability. If nd frequency is tied to depositional environment, then nd frequency should vary according to alluvium, aeolian, and colluvium.

Another possibility is that nd concentrations correlate with changes in atmospheric dynamics during climate shifts. Because the elevated nd counts within the BCI deposits are found in sediments dating to the initial YDB, similar climate reversal events require analysis. The beginning of some of these events corresponds to increases in global wind-blown dust, which increases the mobility of several chemical constituents and the addition of atmospheric components to soil and sediment surfaces. On the basis of an increased abundance in several chemical species found in the U.S.-Greenland Ice Sheet Program (GISP2) Ice Core, Mayewski and colleagues (25) suggested a more dynamic atmosphere during the time of the YD. Could this have resulted in the elevated amounts of nds found in soils of the YD? Several other climatic cycles are thought to have resulted in increased atmospheric dynamics throughout the late Pleistocene and early to mid-Holocene. The fluxes of other atmospheric components also suggest that the Last Glacial Maximum (LGM) and the earliest part of the deglaciation (∼18–15 ka) had similar atmospheric conditions as the YD (25). Do soils from this period also contain elevated amounts of nds? What about other similar soils from other climatic events, such as the 8.2-ka event, which also shows evidence of elevated atmospheric circulation (26), or those represented by DO cycles and Heinrich events, some of which show elevated atmospheric dust concentrations depending on location (e.g., refs. 25–27)? Soils from these periods are present within the BC drainage area. Investigating sediments associated with one or more of these climatic shifts explores the possibility that climatic shifts somehow concentrated nds.

Sample Selection. Bull Creek is characterized today as an intermittent stream, containing a meandering channel bounded by terraces of decreasing elevation and age. The oldest and highest terrace (T-5) contains sediments dating back to the late Pleistocene incision of the BC channel. The basal gravels and sands are consistent with regional incisions defined in other central and southern Plains drainages (28, 29). The BC sequence begins with late Pleistocene channel incision and initial deposition of sands and gravels from a fit, perennial stream. Later deposition belies increasingly underfit stream flow corresponding to increased regional aridity. Alluvial deposition is replaced with aeolian deposition. This general sequence is consistent with regional depositional reconstructions (29, 30).

The chronology for this study was provided by radiometric assay of total carbon from buried soils described at cutbank exposures along the lower reaches of BC, including the BCI exposure (*SI Appendix*, Table S1.1). Soil carbon contains a mixture of recent carbon from bioturbation, carbon introduced into the soil by pedogenesis, and old carbon resident in the deposited sediments. This mixture of carbon sources yields radiocarbon ages that are inexact and occasionally produce age reversals (*SI Appendix*, Table S1.1). However, when combined with regional sedimentologic, pedologic, biologic, and cultural chronologies, these ages can identify important shifts and trends, including the timing of the YD. The shift from alluvial to aeolian deposition at ∼8,670 ± 90 RCYBP (midsoil) in the BCI profile and at 8,200 ± 60 RCYBP (age at burial) at the Leavengood profile corresponds to regional patterns of increased aridity marked by aeolian deposition (28, 29). Radiocarbon ages were also cross-checked with cultural chronologies and biostratigraphy (18, 19; *SI Appendix*, Table S1.1). The presence of an early Paleoindian age cache attributed to the Clovis culture (19) supports the pre-11,000 RCYBP age for the basal sands and gravels found below the lowest BCI T-5 soil. The late Pleistocene age for the lowest T-5 soil is further supported by the latest occurrence of mammoth remains in the BC valley (18). The only large Rancho La Brean species to survive the late Pleistocene extinctions was *Bison antiquus*, which continues to be seen in BC deposits dating up to and including ∼9,000 RCYBP (31). The chronological distribution of taxa within BC is consistent with regional biostratigraphy (32, 33).

In sum, the radiocarbon assay of bulk carbon from buried soil A horizons and associated cultural and faunal materials provide a late Pleistocene/YD chronology that can be tracked along the BC drainage and that is consistent with regional studies (28, 29, 30, 34).

Previous investigations along BC and within the general Beaver River drainage of the Oklahoma panhandle identified an environmental sequence including the LGM, a YD signature comparable to the GISP2 results (*SI Appendix*, Fig. S1.2) (18, 35), and deposits correlating to other defined environmental events. The mapping of terraces (*SI Appendix*, Figs. S1.3 and S1.4) along the lower portion of the BC drainage identified the BC depositional environment at specific temporal settings. Correlating the depositional sequences found in the various terraces with environmental, pedologic, and lithostratigraphic criteria resulted in the selection of 49 samples for nd extraction and characterization.

Samples for this project were selected from the BCI locality that originally yielded cubic diamonds and n-diamonds (4). Kennett and colleagues (4) found a concentration of nds (both n- and cubic forms) centered on the boundary between two soil A horizons interpreted to be the YDB and equivalent to our samples BC20 and BC21. Samples from this profile range from just before ∼11,000 RCYBP (10,870 +/− 132 y for 20 cm of deposition at an estimated rate of 66 y per 10 cm) to today in a series of alluvial and aeolian deposits containing 10 stacked buried soils (*SI Appendix*, Table S1.2). All levels from just below the ∼11,000 level (YDB) to the modern surface were included in this analysis. In addition, select samples from the Hearth locality, located 0.5 km downstream from BCI, were analyzed. A total of six alluvial samples straddle a cultural layer containing a hearth that provided a radiocarbon age on charcoal of ∼2,540 RCYBP.

Table 1. Results and distribution of nanodiamond analysis

Profile and level	Kennett et al. (4), ppb	ND, ppm	Climate change	Anth*	Age, RCYBP	Depth cmbs
BCI						
BC52		190	Late H		0	0–10
BC51		190	Late H	X	<3,000	10–20
BC50		0				20–26
BC49		0				26–36
BC48		0				36–46
BC47		0	Mid H			46–55
BC46		0	Mid H		6,200 ± 90	55–65
BC45		0				65–77
BC44		0			7,660 ± 80	77–87
BC43		0	8,200			87–97
BC42		0				97–104
BC41		0				104–114
BC40		0			8,670 ± 90	114–124
BC39		0				124–134
BC38		0.45				134–144
BC37		0				144–151
BC36		1.9	PBA		9,850 ± 90	151–161
BC35		0.8				161–171
BC34		0.45				171–179
BC33		0				179–189
BC32		0				189–199
BC31		0	YD		10,410 ± 70	199–210
BC30		0	YD		10,400 ± 120	210–220
BC29		0	YD	X		220–230
BC28	5	0	YD		10,750 ± 70	230–238
BC27		0	YD		10,850 ± 210	238–246
BC26		0	YD			246–252
BC25		0.45	YD		10,640 ± 70	252–262
BC24	3	1.9	YD		10,350 ± 210	262–269
BC23		1.9	YD			279–289
BC22		0	YD		10,870 ± 70	289–298
BC21	100	1.9	YDB		11,070 ± 60	298–307
BC20	90	190	YDB			307–312
BC19	1	0				341–351
Hearth						
22		0.45				100–110
21		0				110–120
20		0				120–132
19		0.45	Late H	X	2,540 ± 40	132–142
18		0				142–153
17		0.45				153–164
Leavengood						
18		1.9				285–292
19		1.9	YD		10,330 ± 70	302–310
20		0.45				331–341
21		0	B/A		12,550 ± 70	365–375
22		1.9				387–399
23		0	DO1			399–405
Blue Mound						
22		0				885–895
23		0	LGM			935–945
24		0	LGM		18,000 ± 70	1,000–1,010

*Anth refers to cultural material associated with these levels. B/A, Bolling/Allerod; DO1, Dansgaard-Oeschger 1; H, Holocene; LGM, Latest Glacial Maximum; PBA, PreBoreal/Atlantic; YD, Younger Dryas, YDB, Younger Dryas Boundary.

The hearth is 3 m downstream from the described and sampled profile. The Hearth site samples represent the late Holocene. Also sampled was the Leavengood profile, a T5 remnant 2 km upstream from BCI. At Leavengood, six samples from a continuous column were collected. This locality has two dated soils, one at ~12,550 RCYBP and another at ~10,330 RCYBP (Table 1). These samples provide the DO1, Bolling/Allerod (B/A), and YD intervals. The last locality included in this study is the Blue Mound site, which is located 5 km east and 8 km south of BCI. Blue Mound is a large dune atop a playa that dates to the LGM. Two samples are from ~18,000-y-old playa deposits, and the third is from the basal aeolian deposit.

Results

Initial observation of BC digestion residues identified carbonaceous grains with irregular boundaries and diameters of several hundred nanometers. The lack of expected 2–20-nm grains in our samples prompted us to apply a sample preparation strategy that maximized the possibility for capturing these types of grains. Digestion residues were centrifuged at 1,111 × *g* for 30 min, with the transmission electron microscope (TEM) grid placed in the bottom of the tube (*SI Appendix*, section 2.3). This technique yielded carbonaceous grains in the 2–20-nm size. Examination of the crystalline nanoparticles by high-angle annular dark-field imaging (Fig. 1*A*), high-resolution transmission electron microscopy (HRTEM) (Fig. 1*B*), electron diffraction (Fig. 1*C*), and energy dispersive X-ray analysis demonstrated that the particles were consistent with n-diamonds. Fast Fourier transforms of the lattice fringes from HRTEM images (e.g., *SI Appendix*, Fig. S3.7) exhibited spacings of 2.02–2.08 Å, 1.78–1.85 Å, and 1.03 Å, consistent with n-diamond (e.g., *SI Appendix*, Table S3.1) (36). X-ray analysis detected only carbon with minor amounts of oxygen from regions of the sample containing the smaller particles sitting on the support film, but hydrogen cannot be detected with this method.

After initial identification of n-diamonds, fresh TEM grids were prepared for all samples with the high-speed centrifugation method. Similar n-diamond particles were subsequently found in several other samples, typically with similar overall morphologies. Nanodiamond internal textures were observed with HRTEM. Lattice fringes often cross entire grains, providing evidence that these crystals are not mixtures of disordered graphite, graphene, and graphane, as observed in other natural and anthropogenic nanoscale carbons (e.g., refs. 37–42). A number of other internal textures were observed. These include "star" twins (Fig. 2*A*), thickness/strain fringes, linear twins (Fig. 2*B*), and nonlinear twins. Such twinning has previously been described specifically for diamond (e.g., refs. 43 and 44), including with HRTEM (e.g., ref. 45). In particular, star twins are a unique morphology with a nearly fivefold symmetry. Fivefold rotation symmetry is rare in crystalline materials, as it cannot alone be used to fill space. Star twins have previously been described for diamond (e.g., refs. 14, 46, and 47). Although they can occur in other nanoparticulate materials such as metals (e.g., ref. 48), observation of these twins in multiple samples with carbonaceous grains supports the identification of diamond. Daulton and colleagues (49) observed similar linear and star twins in detonation nd, chemical vapor deposition (CVD) diamond, and meteoritic diamond. The relative abundance of textures was found to be similar for meteoric and CVD diamonds, suggesting that an analogous process to CVD was responsible for the growth of meteoric diamonds. Because of the relatively small proportion of grains observed with HRTEM in each of our samples, no such interpretation could be made.

Nanodiamond grain sizes are mostly limited to <15 nm (*SI Appendix*, Table S2.2). This is consistent with research demonstrating that H-stabilized nd is thermodynamically preferred over graphite in at least part of this size range (50). Peng and colleagues (51) observed a distinct size difference in nds experimentally produced by high-energy carbon implantation in quartz; 5–7-nm diamonds formed at low doses of carbon were cubic, whereas 8–13-nm grains formed at higher doses were n-diamond. Perhaps the incorporation of hydrogen accommodates additional strain, increasing the stability field of nd. Indeed, the phase transition of graphite to nd occurs at lower (pressure/temperature) conditions for nanoscale particles (52). The large grains initially found

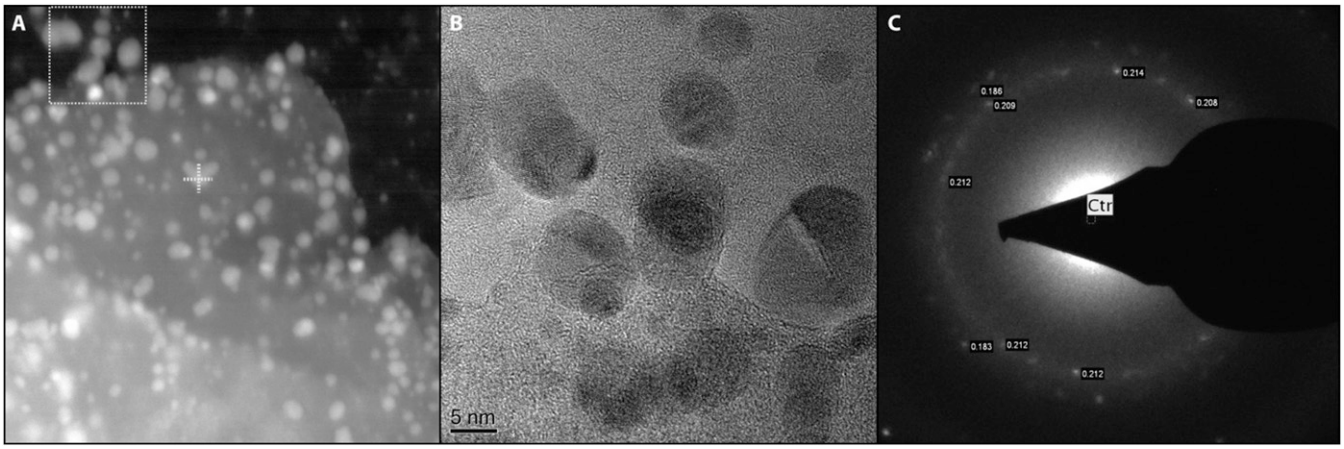

Fig. 1. (*A*) High-angle annular dark-field imaging, (*B*) lattice fringe HRTEM, and (*C*) SAED images collected from an area on the edge of the large single particle in *A*. The area in *B* corresponds to the dashed box in *A*. The cross in *A* corresponds to the point of EELS analysis presented in the *SI Appendix*, Fig. S3.6.

in our study generally appeared analogous to hex nds identified at other sites (11; *SI Appendix*, Fig. S3.1). These grains were almost always aggregates of many subgrains, as evidenced by ring patterns in electron diffraction; however, electron diffraction and electron energy loss spectroscopy (EELS) analyses (*SI Appendix*, Fig. S3.2) demonstrated that these grains were graphene/graphane, as previously suggested by Daulton and colleagues (12). No hex nds were found in BC deposits.

Discussion

Implications of Diamond Investigations for the Impact Hypothesis. Our investigation of BC sediments identified nds primarily as the n-diamond structural form. Bull Creek grains similar to hex diamond (11) were more consistent with graphene/graphane. Diamonds can form in extraterrestrial environments and are present in certain types of meteorites and impact-associated rocks. Two points should be clarified to understand the implications of these observations. First, the n-diamond structure can be considered the same as the cubic structure, but with partial carbon occupancy, hydrogen substitutions, and/or defects that allow the electron diffraction position {200} reflections to appear. Indeed, n-diamonds can form in the laboratory under very similar conditions to those under which cubic diamonds form, including through CVD processes (53, 54). CVD diamond growth has also been identified directly for diamonds associated with meteorites and presolar grains (49). As a consequence, n-diamonds and cubic diamonds can form in terrestrial and extraterrestrial processes. Both n-diamonds and cubic nds were previously identified at BCI (4).

In contrast, the hex diamond structure is significantly different and has been found in nature only in rocks or meteorites that experienced very specific pressure and temperature conditions resulting from shock-conversion of graphite (e.g., ref. 55). Thus, hex diamonds are most likely to be found associated with impact sites (e.g., craters) and not necessarily distributed widely. In fact, a majority of diamonds associated with impacts are of cubic, not hex, form (e.g., refs. 55–58). For example, perhaps the most well-known impact at the Cretaceous–Tertiary boundary formed a well-studied sedimentological layer. Cubic nds were found in multiple investigations of acid-resistant residues of this K–T boundary layer sediment (e.g., refs. 56 and 58). Carbon and nitrogen isotopic signatures of K-T nds indicated they were likely produced on Earth through the impact itself or through interactions of the resulting fireball with the atmosphere (e.g., ref. 59). Similar conclusions were determined for the isotope ratios of nds in YD-equivalent sediments (14). No n-diamonds were reported from the K–T boundary layer, but knowledge of n-diamond at that time was limited, and the authors may have considered any diamonds exhibiting the forbidden reflection as merely a defect version of cubic diamond. Indeed, some authors report that impact diamonds include "highly defective" cubic structures (e.g., ref. 60). Thus, although the presence of hex diamonds is a strong positive indicator of an impact event, the lack of hex diamonds, as in the BCI case, cannot be used to negate the possibility of an impact; instead, it suggests that the point of impact is not nearby.

Nanodiamond Distribution in Space and Time. The search for nds in 49 samples ranging in age from the LGM (ca. 20,000 y ago) to modern times also included samples representing YD-like environmental perturbations, sediments of alluvial and aeolian process, differing periods of surface stability, differing pedologic horizonations, and possible associations with anthropogenic activity. The distribution of samples can be categorized thus: two (4.1%) represent the LGM, one (2%) represents the DO1, one (2%) represents the B/A, two (4.1%) represent the YDB, 11 (22.4%) represent the YD, one (2%) represents the PBA, one (2%) represents the 8.2-ka event, two (4.1%) represent the mid-Holocene, and three (6.1%) represent the late-Holocene periods of climate reversals and periods of increased atmospheric particles (Table 1). The remaining samples (n = 25; 51%) are distributed throughout periods of climatic stability.

Thirty-three (67.3%) of the 49 samples are from alluvial depositions, whereas 16 (32.7%) are aeolian. A total of 37 samples (75.5%) are soil A horizons, 11 (22.4%) are soil B horizons, and 1 (2.0%) is a soil C horizon. Three samples (6.1%) correspond to cultural layers. Nanodiamonds were found in 18 (36.7%) of 49 samples (Table 1). The distribution of confirmed nd occurrences is presented in *SI Appendix*, Figs. S4.1 and 4.2. Nanodiamond quantities range from 1.9 ppm (rank 1), to intermediate level at 1.9–19 ppm (rank 2), and to high concentration of 190 ppm (rank 3;

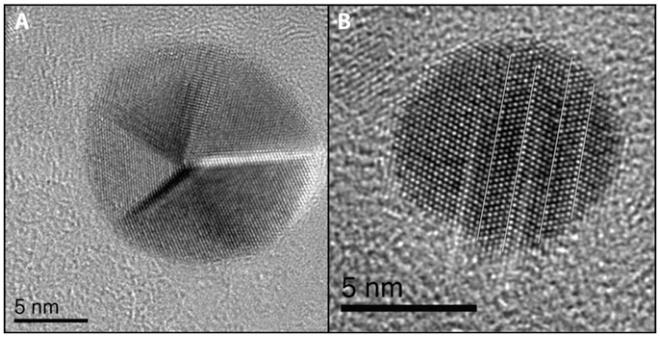

Fig. 2. Nanodiamond textures observed with HRTEM. (*A*) Star twin. (*B*) Multiple linear twins.

SI Appendix, Fig. S4.2). Seven samples fall into rank 1 and eight into rank 2, leaving three of 18 samples (16.7%) in rank 3. It is these three samples that dominate the following discussion.

Eight periods of climatic change accompanied with increased levels of atmospheric particles are represented in the 49 samples of this study. The highest concentrations of nds were only found in two periods, the YDB (n = 1) and Late Holocene (n = 2; Table 1). One of the highest-ranking levels of nd was contained in alluvium, with the remaining two in aeolian deposits, leaving 32 alluvial and 14 aeolian samples without or with low levels of nds. Alluvial samples in the BC1 profile accrued faster than the aeolian samples. If sedimentation rate were a factor concentrating nds, then the slower-accreting aeolian sediments should contain more nds than the alluvial samples. Only three (18.8%) of 16 aeolian samples contained nds compared with 15 (45.5%) of 33 alluvial samples. The low number of both alluvial and aeolian samples with high nd spikes suggests nd accumulation does not correspond to depositional process.

Pedogenesis was not found to be an nd-concentrating factor (*SI Appendix*, Fig. S5.1). Soil A horizons form during periods of relative surface stability in which soil development outperforms sedimentation. Of the three samples with highest levels of nds, two (66.7%) are A horizons; however, these only represent 5.4% (2/37) A horizons. The remaining 94.6% of A horizons did not contain nd spikes.

Nanodiamond concentrations were not correlated with periods of human occupation in the BCI deposits (*SI Appendix*, Fig. S6.1). Distinct cultural zones dated to ∼10,600 RCYBP (level 29), and another at ∼2,000–3,000 RCYBP (level 51), are contained in the deposits. No nd spike accompanies the ∼10,600 RCYBP level. A rank 3 nd spike does, however, occur in the 2,000–3,000-y-old level. Because both cultural layers are replete with hearths and burned lithics and bone, a similar quantity of nds would be expected if this cultural activity were responsible for nd genesis or accumulation.

The nd spike during the 2,000–3,000 RCYBP deposits is enigmatic, first because the nd spike continues beyond the cultural layer to the modern surface, and second because a smaller spike in nd occurrence was identified in the Hearth site deposits of similar age. The Hearth site is a short-term camp dated to 2,540 ± 40 RCYBP. The cultural material included a fire hearth and scatter of tools and bison bone. Sediments from below, at, and above this occupation level were scrutinized for nds. Low quantities (rank 1) of nds were found in three of six samples, but only one sample corresponds to the level of cultural occupation (Table 1). Although this distribution suggests that human activity did not promote the accumulation of nds, the possibility exists that perhaps whatever generated the high nd spike at BCI in a soil A horizon in aeolian deposits is also reflected in the measurable background level of nds in the faster-accruing alluvial deposits at the Hearth site of contemporaneous age to the BCI deposits.

If the YDB and late Holocene concentrations cannot be attributed to specific depositional environments, pedogenesis, periods of environmental perturbations or stability, or cultural activity, then some other n-diamond-producing or concentrating event or condition must have been present at these two times. If an ET source or trigger is to be considered for the YDB spike in nds, then similar consideration would be needed for the late Holocene spike. Searching for such an event is beyond the scope of this article. However, many late Holocene impacts have been documented, including one in Kiowa County, Kansas, ∼160 km northeast of the BC area, that left a 15-m-diameter crater and extensive debris field (53, 61).

Conclusion

The goal of this study was to describe the temporal distribution of nds within the BC drainage of the Beaver River in the Oklahoma panhandle and to evaluate that distribution in light of a proposal that nds are a marker for an extraterrestrial impact that initiated the climatic, biologic, and cultural changes of the YD ∼10,900 RCYBP. Kennett and colleagues (4) had previously identified nds in the BCI profile, including high quantities in samples on either side of the YDB, corresponding to BCI samples 20 and 21 of our study. Our study identified a nd spike of 190 ppm immediately below a soil horizon interpreted as the YDB, diminishing to 1.9 ppm immediately above this soil boundary. Kennett and coworkers found quantities of 1.9 ppb at this soil break that were interpreted by them to be the YDB. Our significantly higher concentration is probably the result of the use of flotation rather than mechanical sieving to obtain the nd-bearing fine-grain samples (*SI Appendix*, section 2.2). We did not, however, conclusively identify the cubic form that had previously been identified by Kennett and colleagues (4). We did identify forms consistent with "highly defective" cubic diamonds. Suspected hex diamonds in the BCI deposits were found to be more consistent with graphene/graphane.

Our findings also identified identical high quantities (190 ppm) of n-diamonds in late-Holocene through present-age deposits at BCI. The second spike of n-diamonds indicates that high levels of nds are not unique to the YDB. The implication of this finding is that either a similar process for concentrating diamonds was acting at both times or a similar event that created the spike at the YDB also occurred during the late Holocene. Similar to Kennett and colleagues (4), we also found low to moderate amounts of nds in samples that could represent background levels. However, most (n = 31 samples; 63%) of the deposits yielded no nds, suggesting there is no reliable background level.

In conclusion, the analysis of 49 sediment samples representing various depositional environments, lithostratigraphic, pedogenic, and global climatic settings identified high levels of nds immediately below and just above YDB deposits and in late-Holocene near-surface deposits. Low quantities (<19 ppm) of nds were found in 15 samples distributed in pre- and post-YDB deposits. Although the high concentration of nds at the YDB along BC may support the ET hypothesis, the high concentration of nds identified in late Holocene deposits indicates such levels are not unique to the YDB.

Methods

Sample collection, preparation, and analysis followed protocols provided by Allen West and published in previous articles (4). Carbonaceous materials were extracted from bulk sediments by digestion and flotation. The resultant concentrate was analyzed by various techniques, including TEM, Select area electron diffraction, energy dispersive spectroscopy, EELS, and HRTEM (*SI Appendix*, sections 2 and 3).

ACKNOWLEDGMENTS. Fieldwork was facilitated by Carolyn Leavengood and John Seaman. This article was greatly enhanced by suggestions from Vance Holliday and an anonymous reviewer. This research was funded in part by National Science Foundation Grant BCS-0918044 (to L.C.B., A.S.M., B.J.C., and A.R.S.). Additional support was received from private donations, especially from Courson Oil and Gas, and the EDMAP program of the US Geological Survey. Institutional support was provided by the University of Oklahoma, Oklahoma State University, and the University of California, Santa Barbara.

1. Firestone RB, et al. (2007) Evidence for an extraterrestrial impact 12,900 years ago that contributed to the megafaunal extinctions and the Younger Dryas cooling. *Proc Natl Acad Sci USA* 104(41):16016–16021.
2. Kerr RA (2008) Paleontology. Experts find no evidence for a mammoth-killer impact. *Science* 319(5868):1331–1332.
3. Pinter N, Ishman SE (2008) Impacts, mega-tsunami, and other extraordinary claims. *GSA Today* 18(1):37–38.
4. Kennett DJ, et al. (2009) Nanodiamonds in the Younger Dryas boundary sediment layer. *Science* 323(5910):94–95.
5. Haynes CV, Jr., et al. (2010) The Murray Springs Clovis site, Pleistocene extinction, and the question of extraterrestrial impact. *Proc Natl Acad Sci USA* 107(9):4010–4015.
6. Pinter N, et al. (2011) The Younger Dryas Impact Hypothesis: A Requiem. *Earth Sci Rev* 106(3-4):247–264.
7. van Hoesel A, et al. (2012) Nanodiamonds and wildfire evidence in the Usselo horizon postdate the Allerod-Younger Dryas boundary. *Proc Natl Acad Sci USA* 109(20):7648–7653.
8. Israde-Alcántara I, et al. (2012) Reply to Blaauw et al., Boslough, Daulton, Gill et al., and Hardiman et al.: Younger Dryas impact proxies in Lake Cuitzeo, Mexico. *Proc Natl Acad Sci USA* 109:E2245–E2247.

9. LeCompte MA, et al. (2012) Independent evaluation of conflicting microspherule results from different investigations of the Younger Dryas impact hypothesis. *Proc Natl Acad Sci USA* 109(44):E2960–E2969.
10. Pigati JS, et al. (2012) Accumulation of impact markers in desert wetlands and implications for the Younger Dryas impact hypothesis. *Proc Natl Acad Sci USA* 109(19): 7208–7212.
11. Kennett DJ, et al. (2009) Shock-synthesized hexagonal diamonds in Younger Dryas boundary sediments. *Proc Natl Acad Sci USA* 106(31):12623–12628.
12. Daulton TL, Pinter N, Scott AC (2010) No evidence of nanodiamonds in Younger-Dryas sediments to support an impact event. *Proc Natl Acad Sci USA* 107(37):16043–16047.
13. Kurbatov AV, et al. (2010) Discovery of a nanodiamond-rich layer in the Greenland ice sheet. *J Glaciol* 56(199):747–757.
14. Tian H, Schryvers D, Claeys P (2011) Nanodiamonds do not provide unique evidence for a Younger Dryas impact. *Proc Natl Acad Sci USA* 108(1):40–44.
15. Daulton TL (2012) Suspect cubic diamond "impact" proxy and a suspect lonsdaleite identification. *Proc Natl Acad Sci USA* 109(34):E2242.
16. Israde-Alcántara I, et al. (2012) Evidence from central Mexico supporting the Younger Dryas extraterrestrial impact hypothesis. *Proc Natl Acad Sci USA* 109(13):E738–E747.
17. Bement LC, Carter BJ (2008) A Younger Dryas Signature on the Southern Plains. *Curr Res Pleist* 25:193–194.
18. Bement LC, Carter BJ, Varney RA, Cummings LS, Sudbury JB (2007) Paleo-Environmental Reconstruction and Bio-Stratigraphy, Oklahoma Panhandle, USA. *Quat Int* 169-170:29–50.
19. Bement L, Schuster K, Carter B (2007) Archeological Survey for Paleo-Indian Sites along the Beaver River, Beaver County, Oklahoma. Oklahoma Archeological Survey Archeological Resource Survey Report No. 54. University of Oklahoma (Oklahoma Archeological Survey, Norman, OK).
20. Bond G, et al. (1997) A Pervasive Millennial-Scale Cycle in North Atlantic Holocene and Glacial Climates. *Science* 278:1257–1266.
21. Bond G, et al. (2001) Persistent solar influence on North Atlantic climate during the Holocene. *Science* 294(5549):2130–2136.
22. Dansgaard W, et al. (1982) A new greenland deep ice core. *Science* 218(4579):1273–1277.
23. Dansgaard W, White JWC, Johnsen SJ (1989) The abrupt termination of the Younger Dryas climate event. *Nature* 339:532–534.
24. Heinrich H (1988) Origin and consequences of cyclic ice rafting in the Northeast Atlantic Ocean during the past 130,000 years. *Quat Res* 29:142–152.
25. Mayewski PA, et al. (1993) Greenland ice core "signal" characteristics offer expanded view of climate change. *J Geophys Res* 98:12,839–12,847.
26. Alley RB, et al. (1997) Holocene Climatic Instability: A Prominent, Widespread Event 8200 Yr Ago. *Geology* 25(6):483–486.
27. Moreno A, et al. (2005) Links between marine and atmospheric processes oscillating on a millennial time-scale. A multi-proxy study of the last 50,000 yr from the Alboran Sea (Western Mediterranean Sea). *Quat Sci Rev* 24:1623–1636.
28. Holliday VT, Meltzer DJ, Mandel R (2011) Stratigraphy of the Younger Dryas Chronozone and Paleoenvironmental Implications: Central and Southern Great Plains. *Quat Int* 242:520–533.
29. Mandel RD (2008) Buried Paleoindian-age Landscapes in Stream Valleys of the Central Plains, USA. *Geomorphology* 101:342–361.
30. Holliday VT (1995) *Stratigraphy and Paleoenvironments of Late Quaternary Valley Fills on the Southern High Plains. Memoir 186* (Geological Society of America, Boulder, Colorado).
31. Bement L, Buehler K, Carter B (2012) Ravenscroft: A Late Paleoindian Bison Kill in the Oklahoma Panhandle. *Oklahoma Anthropol Soc Bull* 60:17–30.
32. Dalquest WW, Baskin JA (1992) Mammals of the Elm Creek Local Fauna, Late Pleistocene of Beaver County, Oklahoma. *Am Midl Nat* 127:13–20.
33. Johnson E (1987) Vertebrate Remains. *Lubbock Lake: Late Quaternary Studies on the Southern High Plains*, ed Johnson E (Texas A&M University Press, College Station), pp 49–89.
34. Haynes CV, Jr. (2008) Younger Dryas "black mats" and the Rancholabrean termination in North America. *Proc Natl Acad Sci USA* 105(18):6520–6525.
35. Bement LC, Carter BJ (2010) Jake Bluff: Clovis Bison Hunting on the Southern Plains of North America. *Am Antiq* 75(4):907–933.
36. Hirai H, Kondo K (1991) Modified phases of diamond formed under shock compression and rapid quenching. *Science* 253(5021):772–774.
37. Bernatowicz TJ, et al. (1996) Constraints on stellar grain formation from presolar graphite in the Murchison meteorite. *Astrophys J* 472:760–782.
38. Fraundorf P, Wackenhut M (2002) The core structure of presolar graphite onions. *Astrophys J* 578:L153–L156.
39. Harris PFJ, Vis RD (2003) High-resolution transmission electron microscopy of carbon and nanocrystals in the Allende meteorite. *Proc R Soc Lond A* 453:2069–2076.
40. Zhu W, Miser DE, Chan WG, Hajaligol MR (2004) HRTEM investigation of some commercially available furnace carbon blacks. *Carbon* 42:1841–1845.
41. Harris PJF (2005) New perspectives on the structures of graphitic carbons. *Crit Rev Solid State Mater Sci* 30:235–253.
42. Croat TK, Stadermann FJ, Bernatowicz TJ (2008) Correlated isotopic and microstructural studies of turbostratic presolar graphites from the Murchison meteorite. *Meteorit Planet Sci* 43(9):1497–1516.
43. Kohn JA (1958) Twinning in diamond-type structures: a proposed boundary-structure model. *Am Mineral* 43:263–284.
44. Shechtman D, Hutchison JL, Robins LH, Farbaugh EN, Feldman A (1993) Growth defects in diamond films. *J Mater Res* 8(3):473–479.
45. van Luyten W, Tendeloo G, Amelinckx S (1992) Electron microscopy study of defects in synthetic diamond layers. *Philos Mag A* 66:899–915.
46. Mani R, Sunkara MK (2003) Kinetic faceting of multiply twinned diamond crystals during vapor phase synthesis. *Diamond & Rel Mat* 12:324–329.
47. Daulton TL (2006) Extraterrestrial nanodiamonds in the cosmos. *Ultrananocrystalline Diamond: Synthesis, Properties, and Applications*, eds Shenderova OA, Gruen DM (William Andrew, Inc., Oxford), pp 23–78.
48. Hofmeister H (2009) Shape variations and anisotropic growth of multiply twinned nanoparticles. *Zeitschriftfür Kristal* 224:528–538.
49. Daulton TL, Eisenhour DD, Bernatowlcz TJ, Lewis RS, Buseck PR (1996) Genesis of presolar diamonds: Comparative high-resolution transmission electronmicroscopy study of meteoritic and terrestrial nano-diamonds. *Geochim Cosmochim Acta* 60:4853–4872.
50. Badzaig P, Verwoerd WS, Ellis WP, Greiner NR (1990) Nanometre-sized diamonds are more stable than graphite. *Nature* 343:244–245.
51. Peng JL, Bursill LA, Jiang B, Orwa JO, Prawer S (2001) Growth of c-diamond, n-diamond and i-carbon nanophases in carbon-ion implanted fused quartz. *Philos Mag B* 81(12):2071–2087.
52. Aleksenskii AE, Baidakova MV, Vul AY, Davydov YV, Pevtsova YA (1997) Diamond-graphite phase transition in ultradisperse-diamond clusters. *Phys Solid State* 39(6): 1007–1015.
53. Wasson JT, Sedwick SP (1969) Possible Sources of Meteoric Material from Hopewell Indian Burial Mounds. *Nature* 222:22–24.
54. Kumar A, et al. (2013) Formation of nanodiamonds at near-ambient conditions via microplasma dissociation of ethanol vapour. *Nat Commun* 4:2618.
55. Hanneman RE, Strong HM, Bundy FP (1967) Hexagonal diamonds in meteorites: implications. *Science* 155(3765):995–997.
56. Carlisle DB, Braman DR (1991) Nanometre-size diamonds in the Cretaceous/Tertiary boundary clay of Alberta. *Nature* 352:708–709.
57. Hough RM, et al. (1995) Diamond and silicon carbide in impact melt rock from the Ries impact crater. *Nature* 378:41–44.
58. Hough RM, Gilmour I, Pillinger CT, Langenhorst F, Montanari A (1997) Diamonds from the iridium-rich K-T boundary layer at Arroyo el Mimbral, Tamaulipas, Mexico. *Geology* 25(11):1019–1022.
59. Gilmour I, et al. (1992) Terrestrial carbon and nitrogen isotopic ratios from cretaceous-tertiary boundary nanodiamonds. *Science* 258(5088):1624–1626.
60. Masaitis VL (1998) Popigai crater: Origin and distribution of diamond-bearing impactites. *Meteorit Planet Sci* 33:349–359.
61. Baillie M (2007) The case for significant numbers of extraterrestrial impacts through the late Holocene. *J Quat Sci* 22:101–109.